Tuneable Metamaterial-like Platforms for Surface-Enhanced Raman Scattering via Three-Dimensional Block Co-polymer-Based Nanoarchitectures

Banbury, Carl; Rickard, Jonathan James Stanley; Mahajan, Sumeet; Goldberg Oppenheimer, Pola

DOI:
10.1021/acsami.9b00420

Document Version
Publisher's PDF, also known as Version of record

Citation for published version (Harvard):
Banbury, C, Rickard, JJS, Mahajan, S & Goldberg Oppenheimer, P 2019, 'Tuneable Metamaterial-like Platforms for Surface-Enhanced Raman Scattering via Three-Dimensional Block Co-polymer-Based Nanoarchitectures' ACS Applied Materials & Interfaces, vol. 11, no. 15, pp. 14437-14444. https://doi.org/10.1021/acsami.9b00420

ACS APPLIED MATERIALS & INTERFACES

Research Article

Cite This: ACS Appl. Mater. Interfaces 2019, 11, 14437−14444

www.acsami.org

Tuneable Metamaterial-like Platforms for Surface-Enhanced Raman Scattering via Three-Dimensional Block Co-polymer-Based Nanoarchitectures

Carl Banbury,[†] Jonathan James Stanley Rickard,[†,‡] Sumeet Mahajan,[§] and Pola Goldberg Oppenheimer*[,†]

[†]School of Chemical Engineering, College of Engineering and Physical Sciences, University of Birmingham, Birmingham B15 2TT, U.K.

[‡]Department of Physics, Cavendish Laboratory, University of Cambridge, JJ Thomson Avenue, Cambridge CB3 0HE, U.K.

[§]Department of Chemistry and the Institute for Life Sciences, University of Southampton, University Road, Southampton SO17 1BJ, U.K.

Supporting Information

ABSTRACT: Surface-enhanced Raman spectroscopy (SERS) pushes past the boundaries and inherent weaknesses of Raman spectroscopy, with a great potential for a broad range of applications particularly, for sensing. Yet, current real world applications are limited due to poor reproducibility, low-throughput, and stability issues. Here, we present the design and fabrication of self-assembly guided structures based on adjustable block co-polymer (BCP) nanomorphologies and demonstrate reproducible SERS enhancement across large areas. Golden three-dimensional (3D) nanostructured morphologies with controllable dimensions and morphologies exhibit high chemical stability, enhanced plasmonic properties and are highly suitable for SERS substrates due to the strong enhancement of the electromagnetic field. Adjustable, free standing porous nanostructures, continuous in 3D space are achieved by removal of selected BCP constituents. Four BCP morphologies and the corresponding achievable enhancement factors are investigated at 633 and 785 nm excitation wavelengths. The choice of excitation laser is shown to greatly affect the observed signal enhancement, highlighting the sensitivity of the technique to the underlying surface architecture and length scales. By using BCP assemblies, it is possible to reliably tune these parameters to match specific applications, thus bridging the gap toward the realization of applied metamaterials. The fabricated SERS platforms via three-dimensional block co-polymer-based nanoarchitectures provide a recipe for intelligent engineering and design of optimized SERS-active substrates for utilization in the Raman spectroscopy-based devices toward enabling the next-generation technologies fulfilling a multitude of criteria.

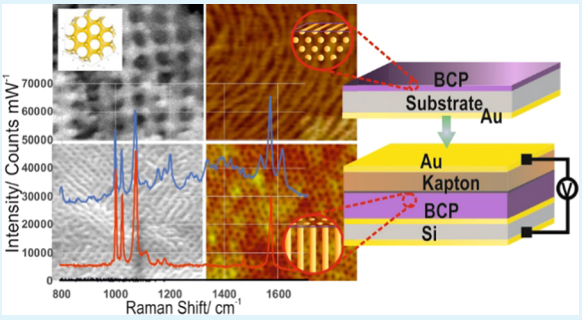

KEYWORDS: *surface-enhanced Raman spectroscopy (SERS), block-co-polymer nanomorphologies, tuneable golden 3D nanostructures*

INTRODUCTION

Block co-polymer (BCP) nanoarchitectures have been emerging as straightforward and high-throughput platforms for designing and fabricating a range of large-area nanostructures with controllable dimensions, composition, and spatial arrangement. Considerable research has been directed toward fabricating and exploiting the self-assembled BCP microphases for their potential implementation into a variety of functional applications, including additives to enable enhanced toughness of plastics and polymer blend composites, guiding the synthesis of nanoparticles[1] acting as capsules for drug delivery,[2] platforms for organic photovolatics, electronics, data storage, and sensors.[3−6] Surface-enhanced Raman spectroscopy (SERS) has been concurrently, a topic of extensive scientific investigations in particular, because of its high-sensitivity and specificity for tracing molecular fingerprints, aided by optically excited localized surface plasmon resonances (LSPRs), yielding intense local electric fields on metal micro to nanostructures.[7−9] A significant SERS enhancement can be achieved via the coupling of the excitations of surface fields to adsorbed or proximal molecules.[10−12] The substrate on which SERS[10,13−21] is performed is often the crucial factor for successful signal enhancement. However, consistent and controllable fabrication of SERS-active, sensitive and adjustable surfaces still remains

Received: January 8, 2019
Accepted: March 18, 2019
Published: March 18, 2019

DOI: 10.1021/acsami.9b00420
ACS Appl. Mater. Interfaces 2019, 11, 14437−14444

challenging. SERS substrates are often limited by instability and lack of tuneability. Since every flaw in the substrate has a direct and considerable impact on the ultimate signal, SERS still requires development of methods for designing, fabricating, and controlling the surface architecture. Many studies exploit nanoparticle-based systems for SERS enhancement and consequently, their reproducibility, stability, and practical applications remain debatable.[22−25] The vast majority of top-down synthetic routes to generate nanostructures are based on conventional patterning techniques and are typically expensive, complex and often require precise integration of multistep processes while exhibiting a limited scalability, highlighting the need for more reliable and straightforward lithographic methods to develop efficient access to adjustable three-dimensionally (3D) isotropic nanostructures. This has driven extensive efforts to explore novel processes for the fabrication of highly ordered 3D structures with sub-micrometer periodicities, signposting BCP self-assembly as an alternative bottom-up lithographic method, enabling specific orientations from chosen materials on supporting substrates, as a platform for a next generation of miniaturized devices. However, the utilization of self-assembled BCPs for plasmonics, including SERS, has only recently begun to gain traction[9,26,27] but still remains predominantly underexplored. Recently, Zhang et al. reported the use of BCP cylinders integrated with silver nanoparticles for enhancing Raman signals,[28] although for practical SERS applications, gold, being more inert and stable, is more suitable than silver. Furthermore, none of the studies has paid attention to the optimization and tuning possibilities, which can be accessed via the range of morphologies of BCP-based substrates for advanced SERS applications. Careful control, understanding, and subsequent intelligent engineering can, therefore, further enable the tailoring of bottom-up BCP morphologies for the generation of "hot-spots"; to take full advantage of the synergistic functions of the resulting BCP-based SERS architectures.

Here, we demonstrate a range of gold SERS-active 3D nanostructures fabricated from block co-polymer self-assembled materials and study their corresponding SERS enhancement and optical properties. Through tailoring the BCP synthesis and tuning the self-assembly, combined with guidance and fabrication of nanomorphologies with characteristic length scales, patterning method and laser frequencies, flexible 3D architectures are fabricated, which are difficult to achieve in another fashion. The fabricated 3D gold SERS substrates are based on block-co-polymer microdomain morphologies and comprised of planar (lamellar) structures, cylindrical (both parallel and perpendicular to the supporting substrates), and gyroid (double and free-standing) morphologies. Selective degradation of the self-assembled phase-separated BCP components, plated with a plasmon-active metal (gold) effectively enhances the electromagnetic field, yielding high SERS signals. Consequently, we have designed nanostructured substrates with varying, laser-matching SERS enhancements, which are known to exhibit different Raman signal augmentation at different excitation wavelengths. Characterization of the photonic properties of 3D BCP-based nano-morphologies revealed that these composite nanostructures behave like new metals with distinct optical characteristics, with a plasma edge shifted to longer wavelengths and a transparency that is greatly increased compared to naturally occurring bulk metal.[29] Substrates with tuneable (controllable) surface plasmon resonances of the nanostructures matching the excitation lasers are essential for gaining the highest enhancements. Broad surface plasmon resonances are needed, especially with red and near-infrared excitation lasers so that high electric fields at both the excitation and Raman scattered wavelengths can be available, to allow for the highest enhancements to be obtained.[30] The obtainable optical properties can be further tuned immensely by variation of the unit cell size, the fill fraction, choice of the BCP morphology, and the plasmonic metal used for filling into the template, building upon the various approaches developed to tune the size, shape, and spacing of BCP domains and the nanostructures derived from them.[31−35] The architectures fabricated here can provide low-cost, simple, large-active-area substrates, with broad plasmon resonances which open a window for a range of SERS active, easily switchable structures to accommodate various applications toward developing novel, adjustable photonic metamaterials and miniaturized devices.

RESULTS AND DISCUSSION

The phase diagram in Figure 1 demonstrates the designed and fabricated BCP assemblies containing a range of nano-

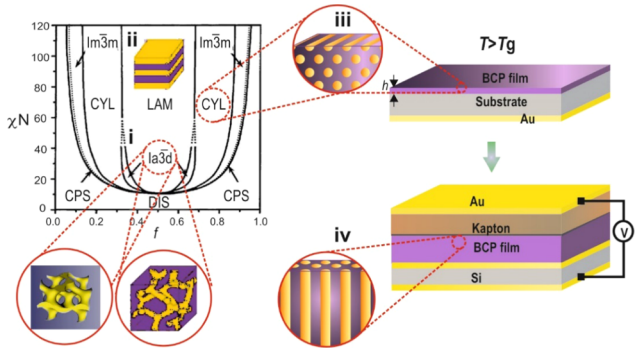

Figure 1. Schematic representation of the fabrication of four morphologies for SERS substrates from the available self-assembled range of BCPs. (i) Three-dimensional gyroid nanostructures comprised of three rotated arms at the 3-fold junction with each arm attached to another set. (ii) Tuning the volume fractions of the blocks yields lamellae and cylinder morphologies. (iii, iv) Fabrication of mixed (hexagonal and lying) cylinder arrays and those perpendicular to the substrate (iv) via annealing of poly(ferrocenylsilane)-*block*-polylactide (PFS-*b*-PLA) film above the glass transition temperature, T_g in a capacitor like set-up with an applied E_f of 155 ± 15 V/μm, which are solidified by quenching to room temperature. Mixed morphology comprised of a combination of parallel and perpendicular to the substrate cylinders can be generated in-between (iii) and (iv) by controlling the strength of the applied electric field.

structured morphologies, including the double gyroid (DG), free-standing gyroid (FSG), mixed combination of parallel and perpendicular to the substrate, (MCYL), hexagonal cylinder domains and only perpendicular cylinders (CYL), accordingly. In the bulk, various morphologies that depend on the relative volume fraction of one block relative to the other produce complex nanostructures due to the microphase separation of the BCPs on the molecular scale resulting in a spontaneous formation of a broad spectrum of ordered nanostructures. The evolving nanomorphologies from the BCP melt are determined by the competition of entropy and the enthalpy between the

DOI: 10.1021/acsami.9b00420
ACS Appl. Mater. Interfaces 2019, 11, 14437−14444

two blocks and eventually result in the minimization of the system's energy, yielding the most favorable configurations.

BCP phase morphology typically evolves at the length scale of tens of nanometers and can be controlled by the volume fractions of the constituent blocks, whereas the total number of monomers N in the BCP chain determines the dimensions of the nanostructure. Lamellar morphology typically results from the alternating symmetric BCP layers, whereas higher levels of one constituting block volume fraction yield asymmetric morphologies comprised of one component forming the minority phase and the other, the matrix phase and finally, with the bicontinuous gyroids (Figure 1i) formed between the lamellae (Figure 1ii) and the hexagonally packed cylinders, oriented parallel to the substrate. BCP self-assembly of random-coil polymers is a highly efficient process and on supporting surfaces, many of the co-polymer morphologies exist naturally in a thin film or layer geometries. However, the interactions of the blocks with the surface typically result in an orientation of the microdomains parallel to the substrate, (Figure 1iii) limiting the successful replication of "lying" cylinders due to the collapse of the structure following the removal of the matrix during the templating process.

Well-defined nanostructures with long-range positional tuning and a high-degree of alignment can be achieved by controlling the hydrodynamic flow and the strength of applied field in a microcapacitor device. Therefore, an experimental set-up for exposing BCP films to an electric field, without a gap, was assembled to perpendicularly align the cylinders lying parallel to the supporting substrate inside the BCP thin film. Application of an external electric field, E_p, enables control of the degree of alignment of the hexagonally ordered cylinders, between lying to perpendicular orientations as well as (between Figure 1iii to iv, accordingly) mixed cylinders morphologies, i.e., MCYL. Annealing above the glass transition temperature of the thin BCP film, without applying an external electric field, results in cylinders which predominantly remain oriented parallel to the substrate with distinctive areas of a terraced-like morphology (Figure 1iii) due to the reorganization of the highly mobile chains in the BCP melt.

Polystyrene-*b*-poly(D,L-lactide) (PS-*b*-PLLA) block-co-polymer was used to synthesize the double gyroid nanostructure comprising two interpenetrating, three-dimensional and continuous networks containing 39% fill fraction (Figure 2a). Selective degradation of the minor phase, while preserving the majority one in a phase-separated block co-polymer morphology, by ultraviolet (UV) ozone etching and via a subtle hydrolytic-degradation, yielded a free-standing gyroid template (Figure 2b), which was subsequently coated with inorganic material such as gold (Figure 3). Thin films (50−400 nm) of poly(ferrocenylsilane)-*block*-polylactide (PFS-*b*-PLA), spin-coated onto a p-doped silicon wafer (covered with a 50 nm gold layer on their backside) or on the fluorine-doped tin oxide (FTO) glass, formed a cylindrical microphase morphology with an ordered block co-polymer containing cylinders of PLA in a matrix of PFS, lying in the plane of the film (Figure 2c). Cylinder orientation parallel to the film's surface is typically thermodynamically preferred because of the differing surface energies of the two blocks at one or both interfaces. The electric field-guided surface morphology of co-polymer cylinders annealed above the glass transition temperature in the capacitor sandwich with an applied voltage of 3−4 kV yielding vertically aligned cylindrical nanodomains parallel to the axis of the electric field lines, (Figure 2d) due to the

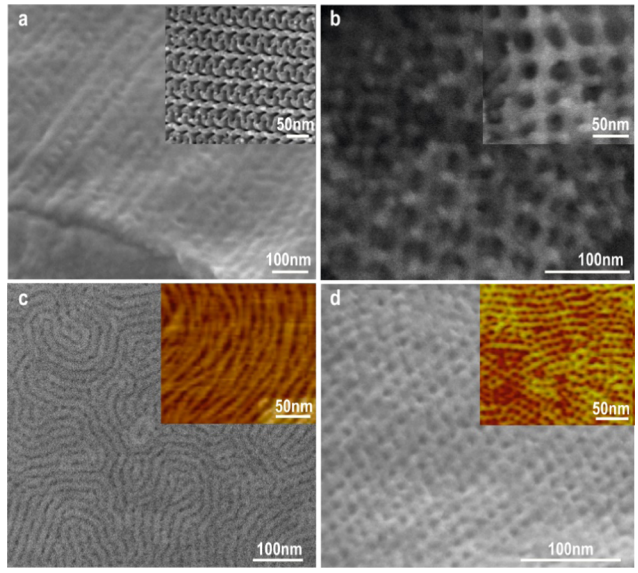

Figure 2. Scanning electron microscopy (SEM) and atomic force microscopy (AFM) characterization of the BCP-based nanomorphologies. Tilted (a) and a top-view (a, inset) images of the initially fabricated DG morphology and (b) FSG nanostructures after the selective removal of the minor phase yielding matrix with interconnected networks as a template for further nucleation and growth of inorganic material. (c) As-spun thin BCP film reveals microphase morphology of lying cylinders (inset) which are then reorganized into vertical cylinders (d) mixed with areas of lying cylinders (MCYL) (d, inset) after the electric field application and annealing in a controlled manner.

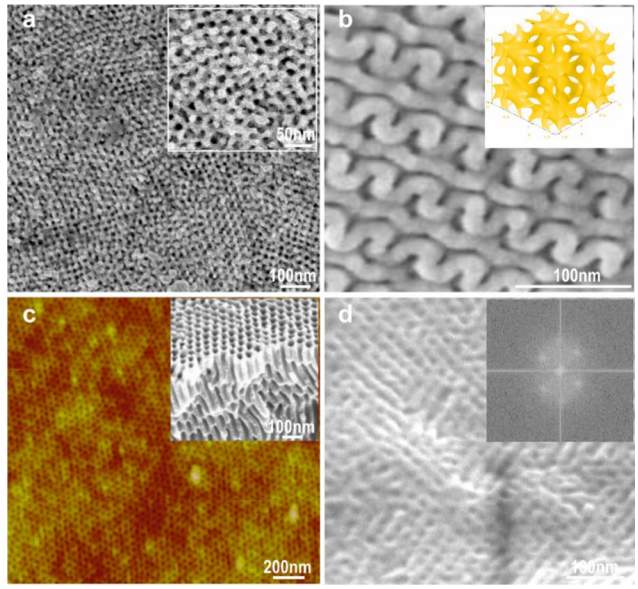

Figure 3. Gold-plated three-dimensional nanomorphologies. Low-angle backscattered scanning electron microscopy (LAB-SEM) images of Au-plated and -sputtered nanostructures of (a) FSG with a unit cell of 20 nm and fill fraction of 21% and (b) DG with the corresponding MATLAB-generated simulations of the nanostructure's cell-unit (inset). (c) AFM height image of aligned cylinders continuously spanning the two electrodes with cross-sectional SEM (c, inset) revealing voids left by removal of the minor phase and subsequently gold plated and sputtered. (d) Surface SEM of the Au-replicated mixed cylindrical morphology after UV ozone etching of PFS matrix with the FFT of the image (inset).

DOI: 10.1021/acsami.9b00420
ACS Appl. Mater. Interfaces 2019, 11, 14437−14444

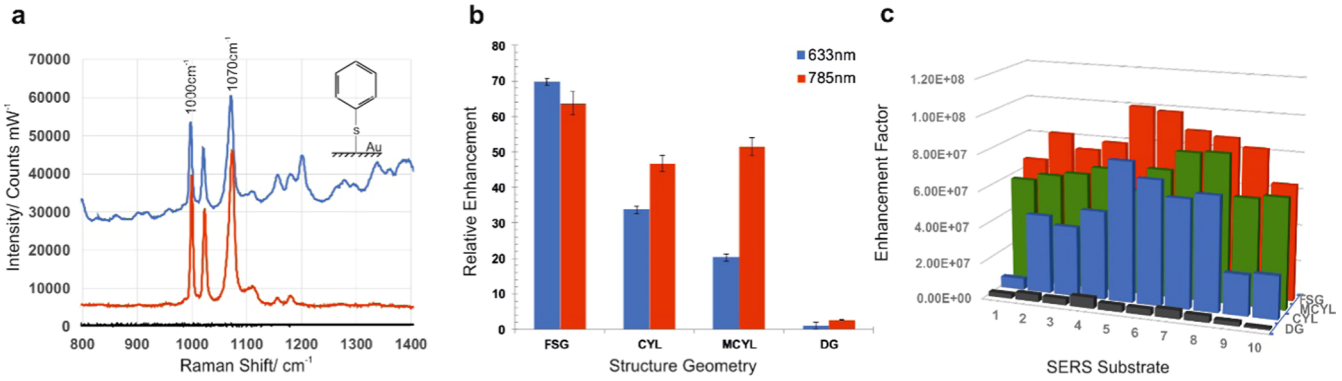

Figure 4. BCP-based SERS substrates. (a) Representative SERS spectra of benzenethiol (inset) recorded from substrates excited with a 633 nm (blue) and 785 lasers (red) with typical Raman bands at 1000 and 1070 cm^{-1} of the aromatic ring deformation vibrations. (b) Relative SERS enhancement of the 1070 cm^{-1} peak with the highest signal enhancement obtained for the FSG with 633 nm followed by MCYL with 785 nm. (c) The average SERS enhancement factors (EFs) of the 3D SERS-active nanomorphologies across 10 areas on each substrate indicate uniform properties across the structured area with EFs of the order of 10^{7-8} for FSG and MCYL and only 10^{5-6} for the DG nanostructures.

fluctuations of the cylinders around their equilibrium positions and reorganization of the annealed microphase morphology toward a higher lateral symmetry. In the assembled micro-capacitor-device geometry, the electric field results in an aligning torque on the BCP cylindrical morphology and enables control and manipulation of the degree and proportion of the alignment yielding the mixed nanomorphology of MCYL (Figures 2d, inset and 3d).[36,37]

Subsequently, a range of gold-plated nanostructures based on branched 3D organic/inorganic nanohybrids was fabricated. Au-plated DG (Figure 3b) and FSG (Figure 3a) interconnected nanonetworks were generated via selective degradation of the PLLA phase and plating with gold (200 ± 30 nm) via electrodeposition or sputtering (see Supporting Information, S1), followed by the UV irradiation, at a wavelength of 254 nm, removing the sacrificial organic layer. Hydrolytic removal of the PLA phase in the cylindrical morphologies and the subsequent electroplating of gold nanolayer, provided topographic cylindrical features, visible in the AFM height and cross-sectional low-angle backscattered scanning electron microscopy (LAB-SEM) images, (Figure 3c and inset) revealing vertically organized cylindrical phase morphologies. Absence or existence of a characteristic frequency in the two-dimensional fast Fourier transform (2D-FFT) power spectrum further helps to identify the lack or existence of the corresponding periodical structural patterns. The lower symmetry of the 2D-FFT power spectrum, corresponding to the experimentally obtained SEM image, pattern in the inset of Figure 3d is indicative of the shorter-range packing in the case of the mixed cylindrical nanomorphologies with a proportion of horizontal and vertical cylinders (Figure 3d).

SERS performance of the four fabricated nanostructures was evaluated through adsorbing a monolayer of benzenethiol, as a Raman probe, from a 10 μM ethanolic solution on each gold nanosurface (Figure 4a) at excitation wavelengths of 633 and 785 nm as well as using rhodamine 6G (R6G) as a Raman active molecule (see Supporting Information, S3).[17,38,39] Notably, SERS spectra of benzenethiol exhibit a difference in intensity of the Raman bands at different excitation wavelengths. Although strong Raman bands at 1000, 1027, and 1070 cm^{-1}, corresponding to the aromatic ring breathing modes, in-plane C−H deformation and rocking vibrations of benzene are observed under excitation of both 633 and 785 nm, at the shorter laser wavelength of 633 nm additional Raman bands, above 1300 cm^{-1} are also enhanced. The absolute enhancement factor (EF) (Figure 4b) for the FSG-based SERS substrate was found to be 6.1×10^7 and 6.7×10^7 at 785 and 633 nm, respectively. For the other three nanostructures of CYL, MCYL and DG, the EF was consistently higher at 785 nm excitation laser with 38% increase in enhancement for the CYL (EF = 4.5×10^7 and 3.2×10^7 at 785 and 633 nm, respectively) and 61% for the MCYL (EF = 5.0×10^7 and 1.9×10^7 at 785 and 633 nm, respectively) in comparison to excitation with a 633 nm laser. The smallest enhancement was observed for the DG based SERS nanostructures with EF of 2.6×10^6 at 785 nm and 9.6×10^5 at 633 nm. The substrates exhibited a good SERS signal reproducibility which was established by examining random areas (n = 10) across each surface under identical experimental conditions using benzenethiol monolayer as the SERS probe, yielding similar relative peak intensities. Uniform and consistent SERS signals were detected from different locations across each sample area as well as across several substrates under identical experimental conditions, with the correlated SERS based enhancement factor calculation, (see Supporting Information, S2) demonstrating that the values are narrowly distributed around the average of $(8.2 \pm 1.2) \times 10^7$, $(4.5 \pm 2.3) \times 10^7$, $6.6 \times 10^7 \pm 8.9 \times 10^6$ and $(3.5 \pm 1.3) \times 10^6$ for FSG, CYL, MCYL and DG, accordingly (Figure 4c). Based on the 0.95 confidence interval data, we therefore expect the difference in enhancement factor as measured between the different areas to lie between (5.8×10^7, 1.1×10^8), (4.6×10^7, 9.0×10^7), (4.9×10^7, 8.4×10^7) and (7.8×10^5, 6.1×10^6) for FSG, CYL, MCYL and DG, respectively. Importantly, all the EFs are on the same order of magnitude of $\times 10^7$ (for FSG, MCYL and CYL) and $\times 10^6$ (for DG) with the small variation in the pre-factor values, with the largest difference in the SERS EFs of less than 7-fold for the DG and less than 2-fold for both the for the MCYL and the FSG (Figure S2), indicating good signal reproducibility in agreement with the typical SERS platforms, considered highly similar even when showing a nearly 1 order of magnitude difference.[40] The EF achieved with these morphologies is of similar or higher magnitude to the commercially available SERS substrates such as for instance, Mesophotincs,[41] ST Japan,[42] Stellnet Inc.[43] as well as to the conventional surfaces reported in literature.[4,44,45]

Interestingly, only for the FSG nanostructure, the relative SERS enhancement of benzenthiol molecules was found to be

DOI: 10.1021/acsami.9b00420
ACS Appl. Mater. Interfaces 2019, 11, 14437−14444

both the highest as well as greater while using the 633 nm laser versus the 785 nm, in comparison to the rest of the nanoarchitectures, for which the 785 nm yielded higher enhancement of the signal relative to the 633 nm. Furthermore, the MCYL SERS surface demonstrated the biggest increase in enhancement using the 785 nm excitation laser versus the 633 nm, greatly exceeding the DG nanostructure, which showed the lowest EF amongst the fabricated substrates (1.9×10^7 compared to 9.6×10^5) (Figure 4b). This can be explained by the fact that SERS enhancement effect is dependent on the wavelength and mainly arises from the LSPRs of the nanoarchitectures and therefore, a particular SERS substrate will exhibit highest enhancement at a certain excitation wavelength. These results indicate that the FSG is the optimal nanostructure to be exploited with the 633 nm excitation laser to yield the highest enhancement. However, since BCP morphologies that are bicontinuous in all three spatial dimensions are still rare and difficult to manufacture in particular, over large areas, the MCYL morphology presents itself as a particularly promising and viable candidate as a strong SERS enhancing substrate with a 785 nm laser. Since the shape of the nano-morphology plays an important role in SERS, and the electromagnetic enhancement is strongly dependent on the surface morphology and precise shape of the features at the metal surface, the optimal SERS enhancement requires a delicate balance between the excited and scattered wavelengths with the plasmon peak of the metal nanostructure. A plasmon which can be excited at the scattered wavelength out-couples the Raman scattered radiation more efficiently. This is important especially in the near-infrared, where the laser excitation and the Raman scattered radiation can be significantly different in terms of wavelength and hence, excitation or existence of plasmonic absorption at one of these is not sufficient for obtaining the highest SERS enhancements. We show that the enhancement factors in SERS are dependent on the excitation wavelength for the same SERS probe molecule even for the same nanostructure. While thiols, such as mercaptobenzoic acid, bind covalently to the gold surface, there has not been any report of contribution of chemical enhancement mechanism in studies using 633 or 785 nm excitation wavelengths[46] except when using semiconductors as substrates.[47] Hence, we can conclude that in this case the electromagnetic enhancement mechanism is the primary reason for the enhancements of 10^5–10^8 observed for the various structures.

While the SERS activity of the plasmonic BCP-morphologies is promising for detection applications due to uniform and high EFs the optical properties of these metamaterials themselves are interesting. New optical properties emerge, different to bulk gold in these metamaterial-like nanostructures. Figure 5 shows the transmittance spectra recorded with unpolarized light in the visible range on each gold-plated nanostructure sample (Figure 5, inset). The spectra are normalized relative to the transmission from a smooth gold film on the same supporting substrate.

For the gold infiltrated nanomorphologies there is a distinct change in the position of the extinction wavelength maximum. For the FSG, a characteristic extinction peak in the transmission is observed around 600 nm, which shifts progressively to higher energy of 485 nm for CYL, 520 nm for MCYL and 540 nm for the DG. The MCYL extinction maximum at 520 nm absorption max is also observed for

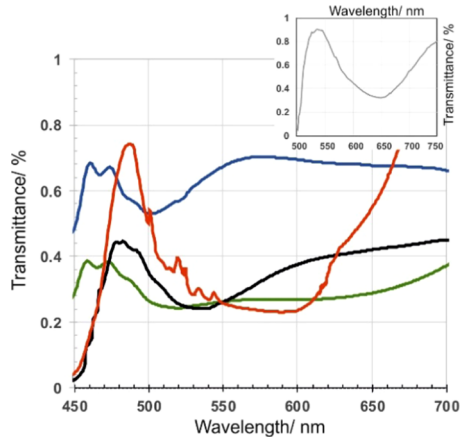

Figure 5. Optical properties of gold-plated nanostructures. Spectroscopic characterization of the optical behavior for transmission configuration with unpolarized incident light for each BCP-based nanomorphology (red: FSG, green: MCYL, blue: CYL and black: DG) with characteristic extinction peaks compared to a gold layer of similar thickness. The blue shift is consistent with what predicted and measured for metamaterials and porous gold and is due to a reduction in the average electron density of the nanostructure and an increase in the self-inductance of the interconnected network of gold.

nanoparticles (20 nm particles) while for bulk gold it is further blue-shifted to 500 nm or below and is related to inter-band transitions, here it is additionally attributable to multi-domain structure as the plasma frequency is inherently modified by the nano-structuring and corresponding air-filling fraction.[48] For single gyroid metamaterials fabricated in gold, properties such as enhanced transmission have been previously observed due to their sub-wavelength architectures and the arising plasmon resonances.[29] The transmission spectrum in Figure 5 of FSG nanostructure is qualitatively similar to that shown for single gyroids previously. The difference in the maximum extinction wavelength at 600 nm compared to the one reported by Salvatore et al.[29] is attributed to the 20 nm unit cell size in the fabricated structures. For DG structures, very low transmission is observed. This is not unsurprising as Hur et al. have previously predicted a different mechanism of propagation of surface plasmons in double gyroid metamaterials.[49] The existence of two interpenetrating continuous plasmon metal networks induces local capacitance and alters the surface plasmon propagation. Thus, losses can be higher and also significantly dependent on each of the interpenetrating structures, e.g., their relative fill-fraction or size of struts. The filling fraction of double gyroid (DG) is higher at 39% than the single gyroid (free standing gyroid; FSG) at 21%. As mentioned by Salvatore et al.[29] and further described by Farah et al.[50] that the reflectivity spectra depend on the structural motifs such as the size of the struts and tune with fill fraction, gyroid pitch and dielectric filling. In our results shown in Figure 5, there is a blue shift of the transmittance-dip between the DG and FSG spectra consistent with the decrease in the filling-fraction. Moreover, the polarization of domains with respect to the incident light can also yield a blue shift of spectra of metamaterials as shown by Vignolini et al.[51] although in our case, we do not expect such differences between FSG and DG films. On the other hand, comparing the spectra for the cylindrical structures we find that the mixed cylinders show two broad peaks while the aligned cylinders show only one peak. This is attributed to the alignment of the

DOI: 10.1021/acsami.9b00420
ACS Appl. Mater. Interfaces 2019, 11, 14437−14444

cylinders with respect to the polarization of the incident (unpolarized) light. In the case of the MCYL the alignment of the cylinders is both perpendicular and parallel to the surface while in the CYL, the cylinders are predominantly perpendicular to the surface. Although an analytical model to predict the extinction peaks is beyond the scope of the current work, we speculate that the broader peak at >600 nm is due to the cylinders parallel to surface (longitudinal mode: along the length) while the peak at ∼500 nm is due to the cylinders perpendicular to the surface (transverse mode). To note, that while the SERS enhancements of the substrates and the optical properties are related, the optical properties of metamaterials, even though fabricated from plasmonic materials, are dominated by those due to their intrinsic structure. Plasmon length scales are of the order of ∼100 nm, while metamaterials such those demonstrated here have <10 nm length scales. The SERS enhancements which are observed in our case provide clear evidence that plasmons are excited in these metamaterials. However, the optical transmission spectra indicate that the optical properties are more than due to plasmonic absorption only with the understanding of the extraordinary optical properties of novel plasmonic metamaterials being an area of active, ongoing research.[52]

CONCLUSIONS

The guided self-assembly of the BCP blocks offers a unique platform for structuring materials with tuneable sizes on the nanoscale thus, offering a great variability of structural features by the independent control of experimental parameters in a robust manner, generating high-fidelity consistent nano-architectures across large substrate areas and subsequently, enabling reliable manufacture of substrates with high SERS enhancements. The optical properties of these nanomaterials are found to be distinguished primarily by the morphology, length scale and periodicity on which the constituent materials are structured. The tuning of plasmon resonances can further be accomplished by controlling the dimensions (size and periods) of the microphase-separated nanostructures, through alteration of the molecular weight and composition which in turn, will allow the design of SERS substrates that generate strong localized electromagnetic fields at optical wavelengths that are required for the optimum SERS excitation by different laser sources thus, harnessing such inherently precise self-assembly behavior of BCPs towards the realization of 3D metamaterials. Dimensional control of the nano-morphologies combined with theoretical modeling could further improve the BCP-based SERS substrates and the enhancements that can be obtained from them and is currently underway. Finally, establishing of such a technique might also provide the missing-link towards the realization of applied metamaterials, heralding a new era for developing novel types of optical materials from BCP self-assembly and their integration into composite functional devices.

EXPERIMENTAL SECTION

Sample Preparation. The samples were prepared using the PFS-*b*-PLA and PS-*b*-PLLA block-copolymers (volume fraction, f = 39%) with thin films spin-coated from a 5−10 wt/wt %, from toluene, onto Au-plated p-doped silicon wafers or transparent FTO glass substrates. The minority component was subsequently removed either by UV etching (15 min at 254 nm) or exposure to plasma system (10 min, O_2 plasma) under controlled low pressure conditions. In order to release the BCP film prior or post degradation and for imaging purposes, the underlying gold layer was removed via etching in 80:1 bromine to methanol solution. The resulting nanostructures were plated via electrodeposition with Au with an initial nucleation step between 0.0 and −1.2 V at a scan rate of 50 mV/s (average of three cyclic voltammetry scans) followed by the deposition step (100 s, −0.8 V) up to a thickness in ranges between 200 and 300 nm.[53] A reaction kinetics-controlled region (from −0.2 to −0.75 V) was followed by a mass transport-controlled region (from −0.8 to −1 V), featuring a cathodic peak characteristic of diffusion-controlled electroplating processes. As the electroplating process was used to obtain nanometer Au layers, the gold growth rate was slow enough to enable careful control over the deposition process, generally achieved in the kinetics-controlled region, where the applied over-potential with respect to the open circuit potential value is small and therefore, acts as the gold deposition driving force. Plating at E = −0.8 V, the electrochemically-driven Au^{3+} reduction occurred at the working electrode with a high deposition rate, leading to the formation of a large number of initial nuclei which ultimately grow to overlap and form a full layer with an average representative thickness of 200 nm (at 100 s deposition time).[54] The nanostructures were alternatively (or additionally) covered with a thin Au film using an Emitech sputter-coater with a direct current Ar plasma (gold target purity 99.999%, Kurt J. Lesker Company) with two cycles of 10 s at 55 mA were carried out.

Alignment of BCP Using an Electric Field. BCP thin film was spin-coated onto a supporting conductive substrate, serving as a bottom electrode, of either silicon with a nanometre gold layer evaporated on the back side of it or FTO glass with a thin layer of silver paste around the edge of the substrate. A capacitor-like device was subsequently assembled with vertical electric field applied across it (a constant high-voltage of 4 kV was applied across the assembled capacitor device), while the BCP film was annealed above the glass transition temperature of both constituent blocks ($T_{g(PFS)}$ = 103 °C and $T_{g(PLA)}$ = 57 °C). The opposing electrode was a 20 μm thick sheet of Kapton with a 50 nm evaporated gold layer on the bottom side along with a thin layer of 2 μm of poly(dimethylsiloxane) (Sylgard 184, Dow-Corning) spin-coated on front of it to establish a conformal contact with the BCP film.

Atomic Force Microscopy. NanoScope IV Multimode and Dimension 3100 (Digital Instruments, Santa Barbara, CA) atomic force microscope were used to thoroughly characterize the surfaces' topography. The AFM measurements were performed using tapping mode via an intermittent contact of the tip with the sample, in ambient conditions. NSG 20 cantilevers with a resonance frequency of 260 kHz and a stiffness of 28 N/m were used. Height and phase images were analyzed with the Nanoscope software (Digital Instruments). To improve contrast, patterns were exposed to UV-light and rinsed in cyclohexane to remove some of the PS phase.

Scanning Electron Microscopy. Samples for SEM imaging were prepared by placing a post-experiment, disassembled substrate with the generated patterns on an inclined or cross-sectional holder to enable the imaging of the top and cross-sectional views. Scanning electron micrographs were acquired using a thermally assisted field emission scanning electron microscope (LEO VP 1530 and FEI Magellan and Helios) with a lateral resolution of 1−5 nm. A LEO ULTRA 55 SEM instrument including a Schottky emitter (ZrO/W cathode) was also used for imaging the samples with a typical acceleration voltage of 2−5 kV equipped with the energy dispersive X-ray spectroscopy. Scanning transmission electron microscope (STEM) images were obtained using Hitachi s5500 with a cold field-emission source and lens detector with 4 Å resolution, allowing adjustable acceptance angle STEM imaging. Low-angle backscattered electron imaging mode was used to contrast the as-spun and those gold replicated samples, providing the atomic number contrast. The power spectrum results of BCP nanostructure images were obtained with the image analysis program (ImageJ) applying a 2D-FFT algorithm.

SERS Measurements. SERS measurements were carried out using micro Raman spectroscopy system with InVia Qontor spectrometer for confocal Raman (Renishaw Plc.) equipped with

DOI: 10.1021/acsami.9b00420
ACS Appl. Mater. Interfaces 2019, 11, 14437−14444

514, 633 and 785 nm lasers which was adjusted for optimal throughput, fluorescence control and sensitivity. Benzenethiol was adsorbed onto the gold surface by soaking in a 10 μm solution in ethanol for 30 min. The samples were then rinsed with ethanol and left to dry in air for 15 min before measurement. The spectra were typically acquired at 10 s exposure time and a laser power of 1−3 mW to avoid photochemical effects in the SERS spectra, sample damage or degradation. SERS maps were generated in a Streamline mode scan with 10 s exposure time and 50 mW power at 633 and 785 nm. A 50× objective with a numerical aperture of 0.75 was used for SERS measurements over a range of 500−1600 cm^{-1} relative to the excitation Raman shift. Optical measurements were carried out with a specially adapted research grade microscope (Leica DM 2700 M) equipped with incoherent white light source, allowing confocal measurements with 2.5 μm depth resolution. The spectra were normalized with respect to those recorded on flat gold or gold covered flat copolymer film surfaces. An intelligent fitting filter was applied for baseline subtraction. After excluding regions with peaks, the baseline was fitted to all the remaining points in each spectrum and a polynomial order of 8 with the noise tolerance of 1.50 was applied.

Optical Characterization. Leica DM200 optical polarizing microscope was used to investigate the optical texture of the samples. The optical transmission characterization of the samples was evaluated in terms of variations of the intensity of transmitted light using unpolarized incident light and the attached spectrometer (Horiba). The microscope xenon lamp acted as an illumination source for the spectroscopic measurements. 100 um optical fiber (ThorLabs) in the focal plane of 20× microscope objective working distance has served as pinhole for the signal collection. Motorized MicroHR Imaging Spectrometer with solid state UV coated silicon over indium gallium arsenide detector for 200−1700 nm and the SynerJY for Windows software were used for data acquisition and analysis.

■ ASSOCIATED CONTENT

Supporting Information

The Supporting Information is available free of charge on the ACS Publications website at DOI: 10.1021/acsami.9b00420.

Thickness characterization of the electrodeposited gold, SERS performance of the BCP-based nanomorphologies using R6G as Raman probe, overview and calculation of the enhancement factor reproducibility (PDF)

■ AUTHOR INFORMATION

Corresponding Author

*E-mail: GoldberP@bham.ac.uk.

ORCID

Sumeet Mahajan: 0000-0001-8923-6666

Pola Goldberg Oppenheimer: 0000-0002-8440-4808

Notes

The authors declare no competing financial interest.

■ ACKNOWLEDGMENTS

We acknowledge funding from the Wellcome Trust (174ISSFPP) and the Royal Academy of Engineering (RF1415/14/28). P.G.O. is a Royal Academy of Engineering Research (RAEng) Fellowship holder. C.B. gratefully acknowledges funding from EPSRC through a studentship from the Sci-Phy-4-Health Centre for Doctoral Training (EP/L016346/1).

■ REFERENCES

(1) Ray, D.; Aswal, V. K.; Kohlbrecher, J. Synthesis and Characterization of High Concentration Block Copolymer-Mediated Gold Nanoparticles. *Langmuir* **2011**, *27*, 4048−4056.

(2) Adams, M. L.; Lavasanifar, A.; Kwon, G. S. Amphiphilic Bock Copolymers for Drug Delivery. *J. Pharm. Sci.* **2003**, *92*, 1343−1355.

(3) Darling, S. B. Block Copolymers for Photovoltaics. *Energy Environ. Sci.* **2009**, *2*, 1266−1273.

(4) Goldberg-Oppenheimer, P.; Kabra, D.; Vignolini, S.; Hüttner, S.; Sommer, M.; Neumann, K.; Thelakkat, M.; Steiner, U. Hierarchical Orientation of Crystallinity by Block-Copolymer Patterning and Alignment in an Electric Field. *Chem. Mater.* **2013**, *25*, 1063−1070.

(5) Park, T. H.; Yu, S.; Cho, S. H.; Kang, H. S.; Kim, Y.; Kim, M. J.; Eoh, H.; Park, C.; Jeong, B.; Lee, S. W.; Ryu, D. Y.; Huh, J.; Park, C. Block Copolymer Structural Color Strain Sensor. *NPG Asia Mater.* **2018**, DOI: 10.1038/s41427-018-0036-3.

(6) Segalman, R. A.; McCulloch, B.; Kirmayer, S.; Urban, J. J. Block Copolymers for Organic Optoelectronics. *Macromolecules* **2009**, *42*, 9205−9216.

(7) Bezares, F. J.; Caldwell, J. D.; Glembocki, O.; Rendell, R. W.; Feygelson, M.; Ukaegbu, M.; Kasica, R.; Shirey, L.; Bassim, N. D.; Hosten, C. The Role of Propagating and Localized Surface Plasmons for SERS Enhancement in Periodic Nanostructures. *Plasmonics* **2012**, *7*, 143−150.

(8) Caldwell, J. D.; Glembocki, O.; Bezares, F. J.; Bassim, N. D.; Rendell, R. W.; Feygelson, M.; Ukaegbu, M.; Kasica, R.; Shirey, L.; Hosten, C. Plasmonic Nanopillar Arrays for Large-Area, High-Enhancement Surface-Enhanced Raman Scattering Sensors. *ACS Nano* **2011**, *5*, 4046−4055.

(9) Hu, W.; Zou, S. Proposed Substrates for Reproducible Surface-Enhanced Raman Scattering Detection. *J. Phys. Chem. C* **2011**, *115*, 4523−4532.

(10) Barnes, W. L.; Dereux, A.; Ebbesen, T. W. Surface Plasmon Subwavelength Optics. *Nature* **2003**, *424*, 824.

(11) Kneipp, K.; Wang, Y.; Kneipp, H.; Perelman, L. T.; Itzkan, I.; Dasari, R. R.; Feld, M. S. Single Molecule Detection Using Surface-Enhanced Raman Scattering (SERS). *Phys. Rev. Lett.* **1997**, *78*, 1667−1670.

(12) Nie, S.; Emory, S. R. Probing Single Molecules and Single Nanoparticles by Surface-Enhanced Raman Scattering. *Science* **1997**, *275*, 1102−1106.

(13) Kho, K.; Qing, Z. M.; Shen, Z. X.; Ahmad, I. B.; Lim, S. C.; Mhaisalkar, S.; White, T.; Watt, F.; Soo, K. C.; Olivo, M. Polymer-Based Microfluidics with Surface-Enhanced Raman-Spectroscopy-Active Periodic Metal Nanostructures for Biofluid Analysis. *J. Biomed. Opt.* **2008**, *13*, No. 054026.

(14) Mahajan, S.; Cole, R. M.; Soares, B. F.; Pelfrey, S. H.; Russell, A. E.; Baumberg, J. J.; Bartlett, P. N. Relating SERS Intensity to Specific Plasmon Modes on Sphere Segment Void Surfaces. *J. Phys. Chem. C* **2009**, *113*, 9284−9289.

(15) Ozbay, E. Plasmonics: Merging Photonics and Electronics at Nanoscale Dimensions. *Science* **2006**, *311*, 189−193.

(16) Pennathur, S.; Fygenson, D. Improving Fluorescence Detection in Lab on Chip Devices. *Lab Chip* **2008**, *8*, 649−652.

(17) Goldberg-Oppenheimer, P.; Mahajan, S.; Steiner, U. Hierarchical Electrohydrodynamic Structures for Surface-Enhanced Raman Scattering. *Adv. Mater.* **2012**, *24*, OP175−OP180.

(18) Rebbecchi, T. A.; Chen, Y. Template-based Fabrication of Nanoporous Metals. *J. Mater. Res.* **2018**, *33*, 2−15.

(19) Bartlett, P. N.; Baumberg, J. J.; Birkin, P. R.; Ghanem, M. A.; Netti, M. C. Highly Ordered Macroporous Gold and Platinum Films Formed by Electrochemical Deposition through Templates Assembled from Submicron Diameter Monodisperse Polystyrene Spheres. *Chem. Mater.* **2002**, *14*, 2199−2208.

(20) Ngo, Y. H.; Li, D.; Simon, G. P.; Garnier, G. Gold Nanoparticle−Paper as a Three-Dimensional Surface Enhanced Raman Scattering Substrate. *Langmuir* **2012**, *28*, 8782−8790.

(21) Santoro, G.; Yu, S.; Schwartzkopf, M.; Zhang, P.; Vayalil, S. K.; Risch, J. F. H.; Rübhausen, M. A.; Hernández, M.; Domingo, C.;

Roth, S. V. Silver Substrates for Surface Enhanced Raman Scattering: Correlation Between Nanostructure and Raman Scattering Enhancement. *Appl. Phys. Lett.* **2014**, *104*, No. 243107.
(22) Lim, C.; Hong, J.; Chung, B. G.; deMello, A. J.; Choo, J. Optofluidic platforms Based on Surface-Enhanced Raman Scattering. *Analyst* **2010**, *135*, 837−844.
(23) Piorek, B. D.; Lee, S. J.; Santiago, J. G.; Moskovits, M.; Banerjee, S.; Meinhart, C. D. Free-Surface Microfluidic Control of Surface-Enhanced Raman Spectroscopy for the Optimized Detection of Airborne Molecules. *Proc. Natl. Acad. Sci. U.S.A.* **2007**, *104*, 18898−18901.
(24) Qian, X.; Zhou, X.; Nie, S. Surface-Enhanced Raman Nanoparticle Beacons Based on Bioconjugated Gold Nanocrystals and Long Range Plasmonic Coupling. *J. Am. Chem. Soc.* **2008**, *130*, 14934−14935.
(25) Ackermann, L.; Andreas, A.; Robert, B. Catalytic Arylation Reactions by C-H Bond Activation with Aryl Tosylates. *Angew. Chem., Int. Ed.* **2006**, *45*, 2619−2622.
(26) Hsueh, H.-Y.; Hung-Ying, C.; Yu-Chueh, H.; Yi-Chun, L.; Shangjr, G.; Rong-Ming, H. Well-Defined Multibranched Gold with Surface Plasmon Resonance in Near-Infrared Region from Seeding Growth Approach Using Gyroid Block Copolymer Template. *Adv. Mater.* **2013**, *25*, 1780−1786.
(27) Wang, Y.; Becker, M.; Wang, L.; Liu, J.; Scholz, R.; Peng, J.; Gösele, U.; Christiansen, S.; Kim, D. H.; Steinhart, M. Nanostructured Gold Films for SERS by Block Copolymer-Templated Galvanic Displacement Reactions. *Nano Lett.* **2009**, *9*, 2384−2389.
(28) Zhang, X.; Lee, W.; Lee, S. Y.; Gao, Z.; Rabin, O.; Briber, R. In *Silver Based SERS Substrates Fabricated from Block Copolymer Thin Film*, APS March Meeting, 2013; p 34006.
(29) Salvatore, S.; Demetriadou, A.; Vignolini, S.; Oh, S. S.; Wuestner, S.; Yufa, N. A.; Stefik, M.; Weisner, U.; Baumberg, J. J.; Hess, O.; Steiner, U. Tunable 3D Extended Self-Assembled Gold Metamaterials with Enhanced Light Transmission. *Adv. Mater.* **2013**, *25*, 2713−2716.
(30) Mahajan, S.; Baumberg, J. J.; Russell, A. E.; Bartlett, P. N. Reproducible SERRS from Structured Gold Surfaces. *Phys. Chem. Chem. Phys.* **2007**, *9*, 6016−6020.
(31) Vriezekolk, E. J.; de Weerd, E.; de Vos, W. M.; Nijmeijer, K. Control of Pore Size and Pore Uniformity in Films Based on Self-Assembling Block Copolymers. *J. Polym. Sci., Part B: Polym. Phys.* **2014**, *52*, 1568−1579.
(32) Radjabian, M.; Abetz, V. Tailored Pore Sizes in Integral Asymmetric Membranes Formed by Blends of Block Copolymers. *Adv. Mater.* **2015**, *27*, 352−355.
(33) Gu, Y.; Wiesner, U. Tailoring Pore Size of Graded Mesoporous Block Copolymer Membranes: Moving from Ultrafiltration toward Nanofiltration. *Macromolecules* **2015**, *48*, 6153−6159.
(34) Guo, T.; Gao, J.; Xu, M.; Ju, Y.; Li, J.; Xue, H. Hierarchically Porous Organic Materials Derived From Copolymers: Preparation and Electrochemical Applications. *Polym. Rev.* **2018**, 1−38.
(35) Dorin, R. M.; Phillip, W. A.; Sai, H.; Werner, J.; Elimelech, M.; Wiesner, U. Designing Block Copolymer Architectures for Targeted Membrane Performance. *Polymer* **2014**, *55*, 347−353.
(36) Crossland, E. J. W.; Kamperman, M.; Nedelcu, M.; Ducati, C.; Wiesner, U.; Smilgies, D. M.; Toombes, G. E. S.; Hillmyer, M. A.; Ludwigs, S.; Steiner, U.; Snaith, H. J. A Bicontinuous Double Gyroid Hybrid Solar Cell. *Nano Lett.* **2009**, *9*, 2807−2812.
(37) Goldberg-Oppenheimer, P.; Eder, D.; Steiner, U. Carbon Nanotube Alignment *via* Electrohydrodynamic Patterning of Nanocomposites. *Adv. Funct. Mater.* **2011**, *21*, 1895−1901.
(38) Biggs, K. B.; Camden, J. P.; Anker, J. N.; Duyne, R. P. V. Surface-Enhanced Raman Spectroscopy of Benzenethiol Adsorbed from the Gas Phase onto Silver Film over Nanosphere Surfaces: Determination of the Sticking Probability and Detection Limit Time. *J. Phys. Chem. A* **2009**, *113*, 4581−4586.
(39) Tian, F.; Bonnier, F.; Casey, A.; Shanahan, A. E.; Byrne, H. J. Surface enhanced Raman scattering with gold nanoparticles: effect of particle shape. *Anal. Methods* **2014**, *6*, 9116−9123.
(40) Ansar, S. M.; Li, X.; Zou, S.; Zhang, D. Quantitative Comparison of Raman Activities, SERS Activities, and SERS Enhancement Factors of Organothiols: Implication to Chemical Enhancement. *J. Phys. Chem. Lett.* **2012**, *3*, 560−565.
(41) Mesophotonics. http://www.mesophotonics.com/products/klarite.html.
(42) Japan, S.T.. http://www.stjapan.de/en/shop/accessories-for-spectroscopy-microanalysis/raman-sers-substrate/).
(43) StellarNet, Inc.. https://www.stellarnet.us/spectrometers-accessories/sers-substrates/.
(44) Srichan, C.; Ekpanyapong, M.; Horprathum, M.; Eiamchai, P.; Nuntawong, N.; Phokharatkul, D.; Danvirutai, P.; Bohez, E.; Wisitsoraat, A.; Tuantranont, A. Highly-Sensitive Surface-Enhanced Raman Spectroscopy (SERS)-based Chemical Sensor using 3D Graphene Foam Decorated with Silver Nanoparticles as SERS substrate. *Sci. Rep.* **2016**, *6*, No. 23733.
(45) Schmidt, M. S.; Hübner, J.; Boisen, A. Large Area Fabrication of Leaning Silicon Nanopillars for Surface Enhanced Raman Spectroscopy. *Adv. Mater.* **2012**, *24*, OP11−OP18.
(46) Michota, A.; Bukowska, J. Surface-Enhanced Raman Scattering (SERS) of 4-Mercaptobenzoic Acid on Silver and Gold Substrates. *J. Raman Spectrosc.* **2003**, *34*, 21−25.
(47) Zhang, X.; Yu, Z.; Ji, W.; Sui, H.; Cong, Q.; Wang, X.; Zhao, B. Charge-Transfer Effect on Surface-Enhanced Raman Scattering (SERS) in an Ordered Ag NPs/4-Mercaptobenzoic Acid/TiO2 System. *J. Phys. Chem. C* **2015**, *119*, 22439−22444.
(48) Dolan, J. A.; Saba, M.; Dehmel, R.; Gunkel, I.; Gu, Y.; Wiesner, U.; Hess, O.; Wilkinson, T. D.; Baumberg, J. J.; Steiner, U.; Wilts, B. D. Gyroid Optical Metamaterials: Calculating the Effective Permittivity of Multidomain Samples. *ACS Photonics* **2016**, *3*, 1888−1896.
(49) Hur, K.; Fracescato, Y.; Giannini, V.; Maier, S.; Hennig, R. G.; Weisner, U. Three-Dimensionally Isotropic Negative Refractive Index Materials from Block Copolymer Self-Assembled Chiral Gyroid Networks. *Angew. Chem., Int. Ed.* **2011**, *50*, 11985−11989.
(50) Farah, P.; Demetriadou, A.; Salvatore, S.; Vignolini, S.; Stefik, M.; Wiesner, U.; Hess, O.; Steiner, U.; Valev, V.; Baumberg, J. Ultrafast Non-linear Response of Gold Gyroid 3D Metamaterials. *Phys. Rev. Appl.* **2014**, *2*, No. 044002.
(51) Vignolini, S.; Yufa, N. A.; Cunha, P. S.; Guldin, S.; Rushkin, I.; Stefik, M.; Hur, K.; Wiesner, U.; Baumberg, J. J.; Steiner, U. A 3D Optical Metamaterial Made by Self-Assembly. *Adv. Mater.* **2012**, *24*, OP23−OP27.
(52) Hess, O.; Pendry, J. B.; Maier, S. A.; Oulton, R. F.; Hamm, J. M.; Tsakmakidis, K. L. Active Nanoplasmonic Metamaterials. *Nat. Mater.* **2012**, *11*, 573−584.
(53) Tucker, R. E. *Universal Metal Finishing Guidebook*; Elsevier: New York, 2014.
(54) Estrine, E. C.; Riemer, S.; Venkatasamy, V.; Stadler, B.; Tabakovic, I. Mechanism and Stability Study of Gold Electrodeposition from Thiosulfate-Sulfite Solution. *J. Electrochem. Soc.* **2014**, *161*, 687−696.

DOI: 10.1021/acsami.9b00420
ACS Appl. Mater. Interfaces 2019, 11, 14437−14444